Electronic Supplementary Information

Graphene－Boron Nitride Hybrid Supported Single Mo Atom Electrocatalysts for Efficient Nitrogen Reduction Reaction

Yan Huang,‡[a] Tongtong Yang,‡[a] Li Yang,[a] Ran Liu,[a] Guozhen Zhang,[a] Jun Jiang,[a] Yi Luo,[a] Ping Lian,*[b] and Shaobin Tang,*[b]

[a] Hefei National Laboratory for Physical Sciences at the Microscale, Collaborative Innovation Center of Chemistry for Energy Materials, Hefei Science Center of CAS, School of Chemistry and Materials Science, University of Science and Technology of China, Hefei, Anhui 230026, P. R. China

[b] Key Laboratory of Organo-Pharmaceutical Chemistry of Jiangxi Province, Gannan Normal University, Ganzhou 341000, China.

Table S1. The formation energies of a boron ($E_{f\text{-}B}$), nitrogen ($E_{f\text{-}N}$) or carbon ($E_{f\text{-}C}$) monovacancy of different BCN-**n** and bare-C.

	$E_{f\text{-}B}$ /eV	$E_{f\text{-}N}$ /eV	$E_{f\text{-}C}$ /eV
BCN-0	9.83	7.76	-
BCN-1	6.65	7.54	7.97
BCN-2	7.22	7.54	9.55
BCN-3	7.22	7.57	9.17
BCN-4	6.78	7.48	9.33
BCN-5	5.64	6.65	8.98
C	-	-	10.26

Table S2. The binding energies of single Mo atom adsorbed on boron ($E_{b\text{-}B}$), nitrogen ($E_{b\text{-}N}$) or carbon ($E_{b\text{-}C}$) defective BCN-**n** and bare-C.

	$E_{b\text{-}B}$ /eV	$E_{b\text{-}N}$ /eV	$E_{b\text{-}C}$ /eV
Mo@BCN-0	8.98	5.16	-
Mo@BCN-1	7.97	5.40	6.78
Mo@BCN-2	8.85	5.16	8.33
Mo@BCN-3	8.38	5.21	7.64
Mo@BCN-4	8.05	5.42	7.76
Mo@BCN-5	7.13	6.04	7.09
Mo@C	-	-	9.02

Table S3. Polarization positive charges of Mo extracted from the boron defective BCN-**n**.

	Mo charge (e^+)
Mo@BCN-0	1.27
Mo@BCN-1	1.27
Mo@BCN-2	1.28
Mo@BCN-3	1.30
Mo@BCN-4	1.29
Mo@BCN-5	1.30

Table S4. The adsorption energies (E_{ads}) of N_2 on different Mo@BCN-**n** with the end-on and side-on configurations.

	E_{ads} /eV	
	End-on	Side-on
Mo@BCN-0	0.70	0.35
Mo@BCN-1	1.04	0.93
Mo@BCN-2	0.84	0.71
Mo@BCN-3	0.77	0.56
Mo@BCN-4	0.80	0.71
Mo@BCN-5	1.13	0.97

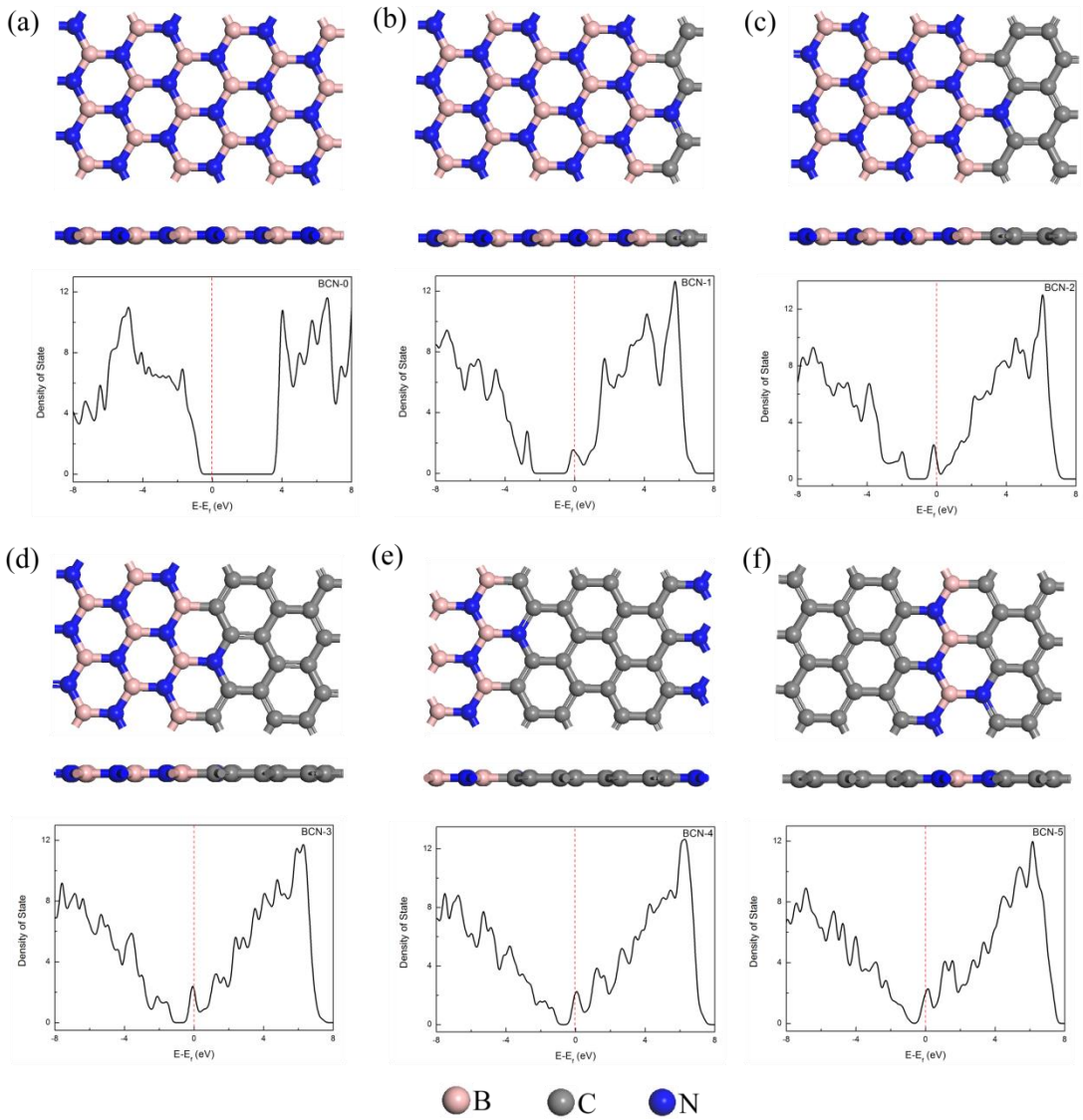

Fig. S1. The optimized structures of different structural models and corresponding density of states of perfect BCN-**n**.(a)-(f) represent BCN-0, BCN-1, BCN-2, BCN-3, BCN-4 and BCN-5, respectively.

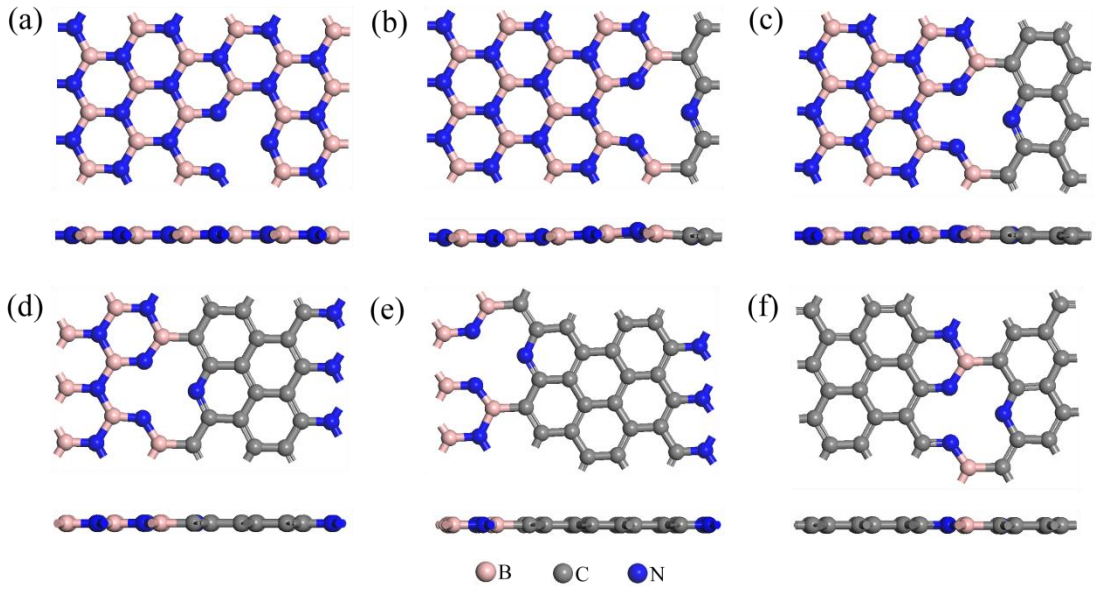

Fig. S2. The optimized structures of defective BCN-**n** with B vacancy. (a)-(f) represent defective BCN-0, BCN-1, BCN-2, BCN-3, BCN-4 and BCN-5, respectively.

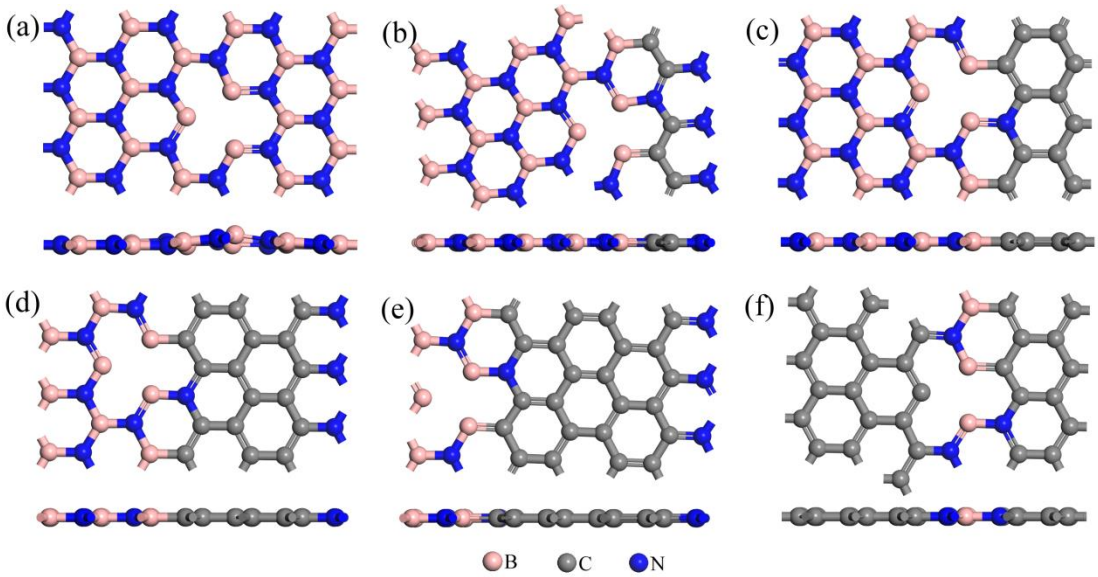

Fig. S3. The optimized structures of defective BCN-**n** with N vacancy. (a)-(f) represent defective BCN-0, BCN-1, BCN-2, BCN-3, BCN-4 and BCN-5, respectively.

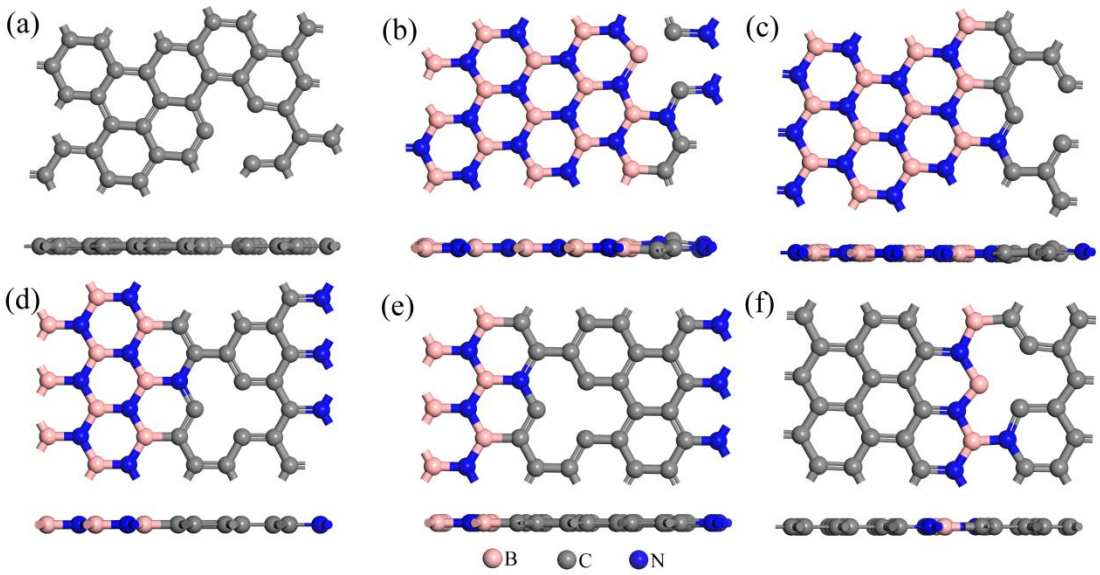

Fig. S4. The optimized structures of defective BCN-**n** with C vacancy. (a)-(f) represent defective bare C, BCN-1, BCN-2, BCN-3, BCN-4 and BCN-5, respectively.

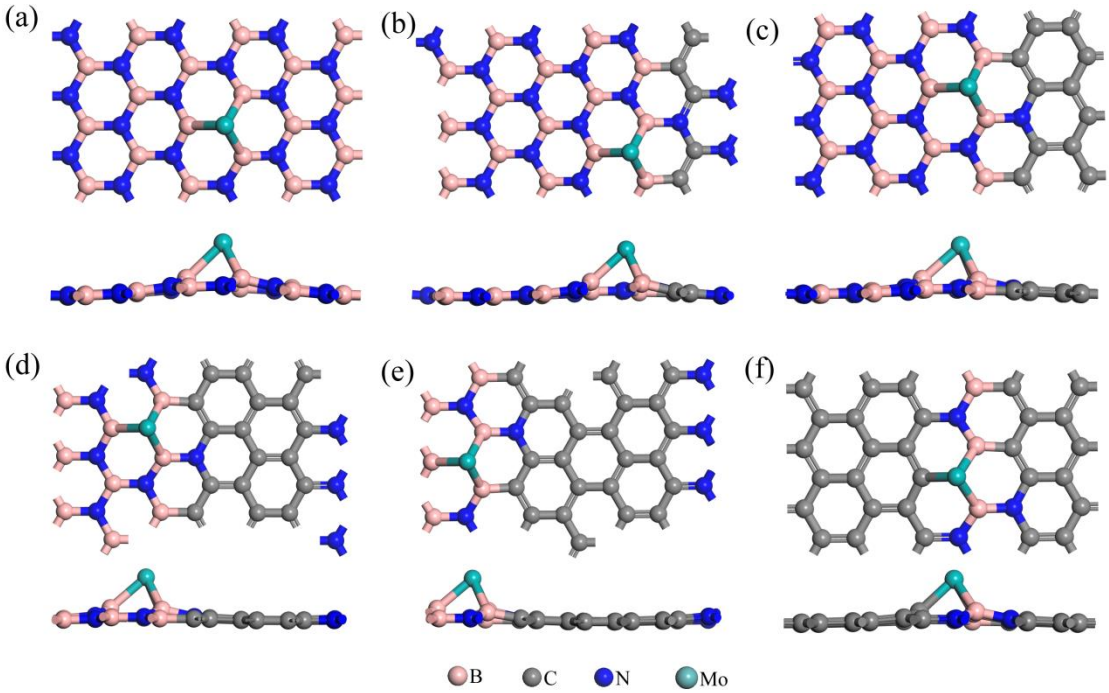

Fig. S5. The optimized structures of Mo@BCN-**n** with Mo was deposited on N vacancy. (a)-(f) represent Mo@BCN-0, Mo@BCN-1, Mo@BCN-2, Mo@BCN-3, Mo@BCN-4 and Mo@BCN-5, respectively.

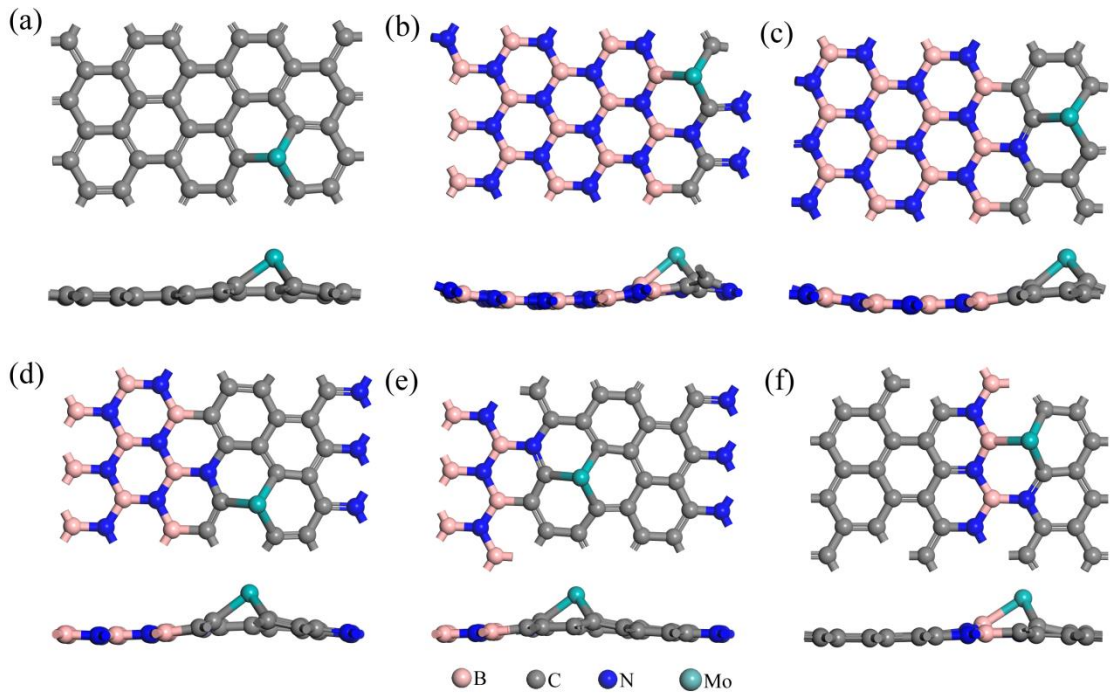

Fig. S6. The optimized structures of Mo@BCN-**n** with Mo was deposited on C vacancy. (a)-(f) represent Mo@C, Mo@BCN-1, Mo@BCN-2, Mo@BCN-3, Mo@BCN-4 and Mo@BCN-5, respectively.

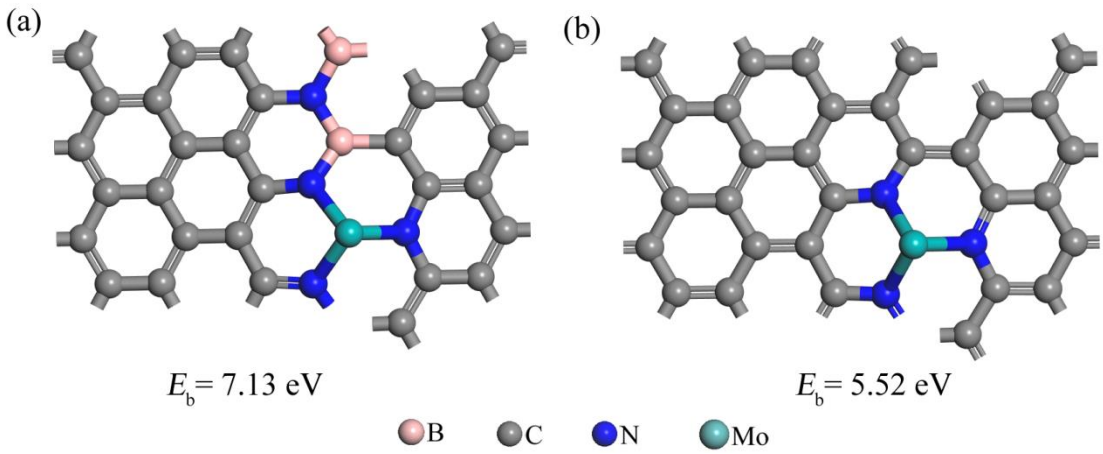

Fig. S7. The geometrical structures for single Mo atom anchored on (a) defective BCN and (b) pyridinic-like N doped graphene and the corresponding binding energy (E_b in eV).

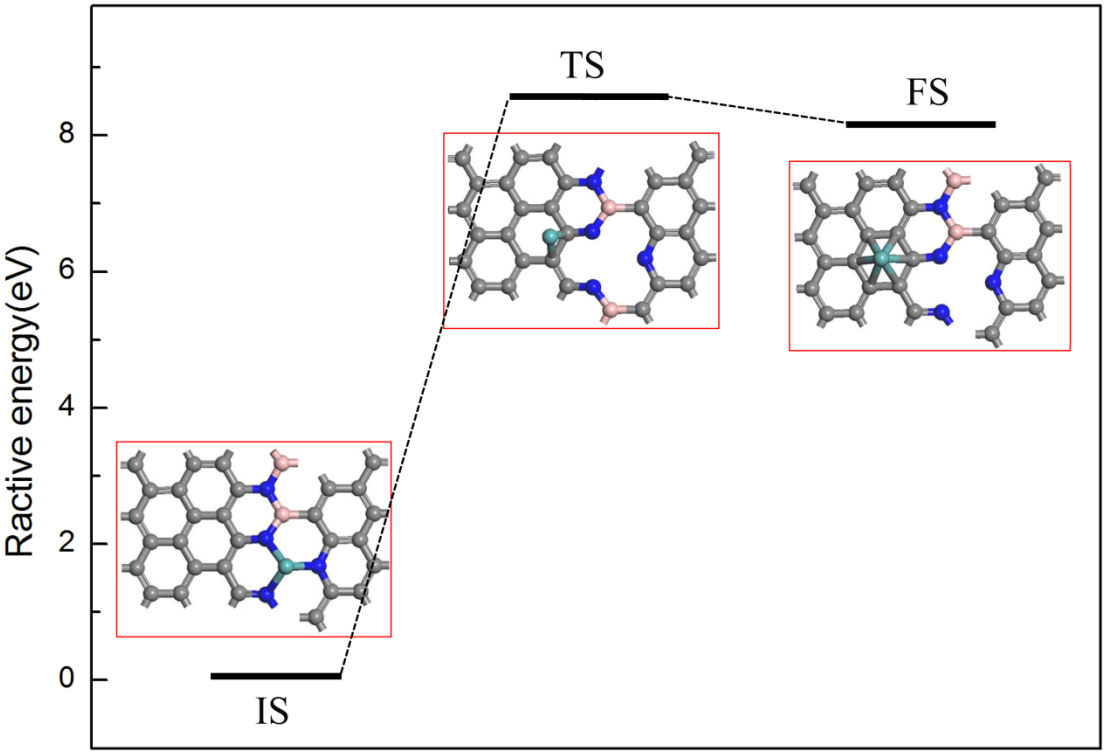

Fig. S8. Potential energy profile for the diffusion of the adsorbed Mo atom from the B defect site to the neighboring hollow site on Mo@BCN-5. From left to right: optimized geometries of initial state (**IS**), transition state (**TS**),and final state (**FS**).

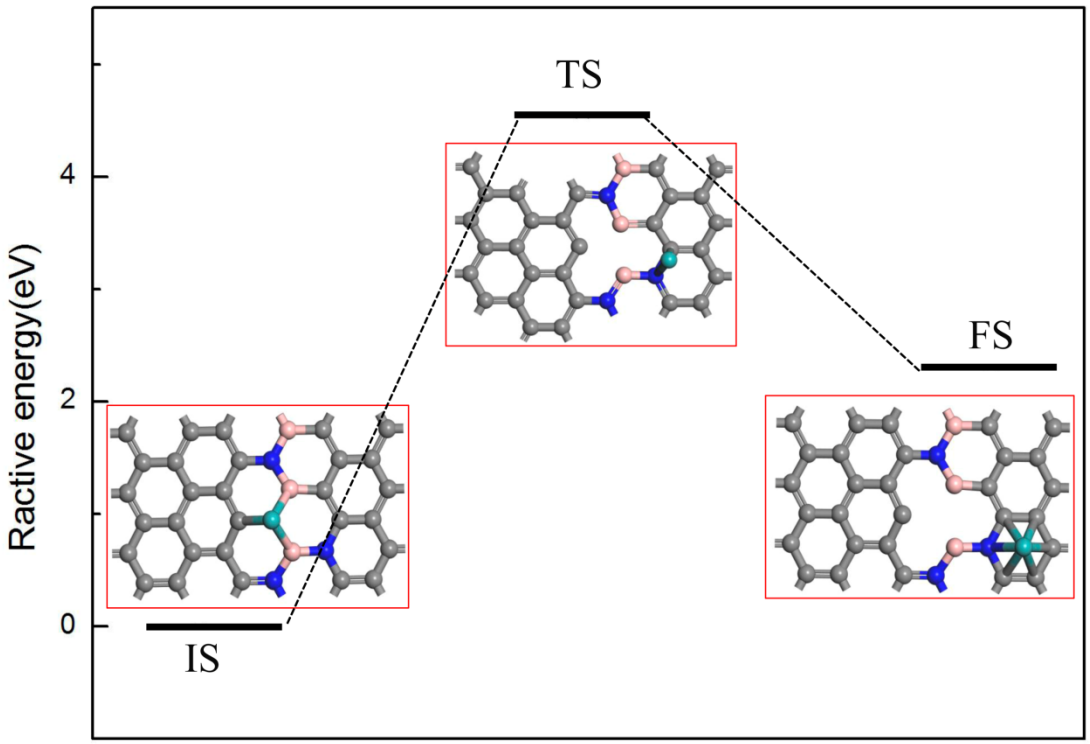

Fig. S9. Potential energy profile for the diffusion of the adsorbed Mo atom from the N defect site to the neighboring hollow site on Mo@BCN-5. From left to right: optimized geometries of initial state (**IS**), transition state (**TS**),and final state (**FS**).

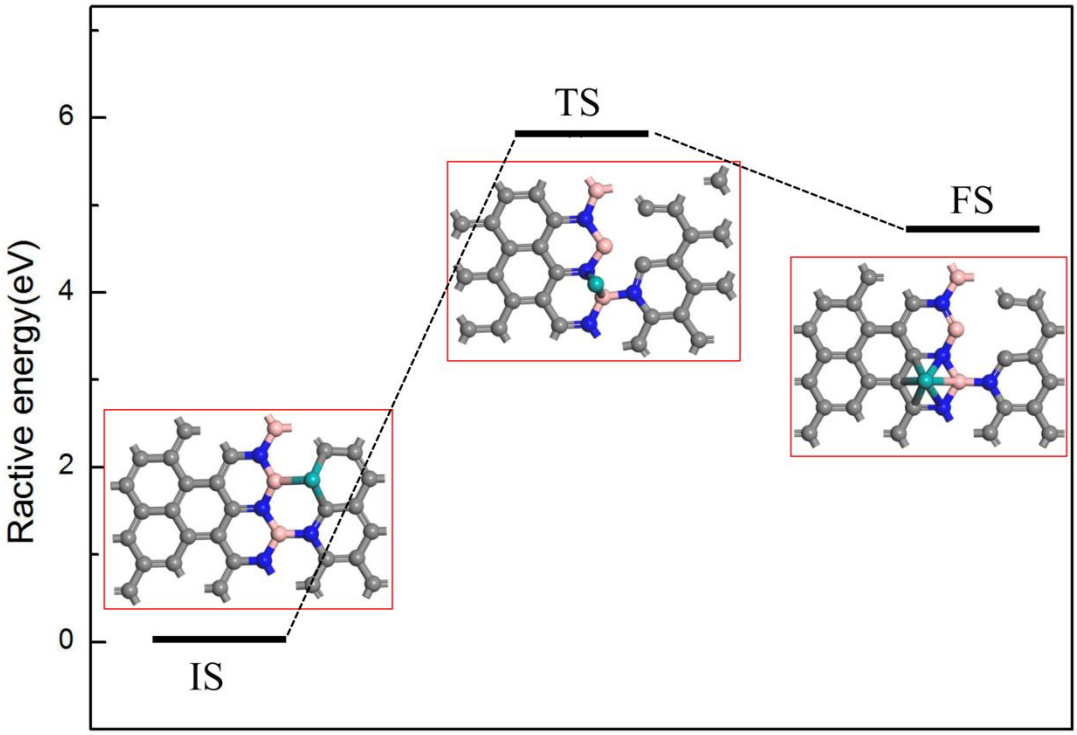

Fig. S10. Potential energy profile for the diffusion of the adsorbed Mo atom from the C defect site to the neighboring hollow site on Mo@BCN-5. From left to right: optimized geometries of initial state (**IS**), transition state (**TS**),and final state (**FS**).

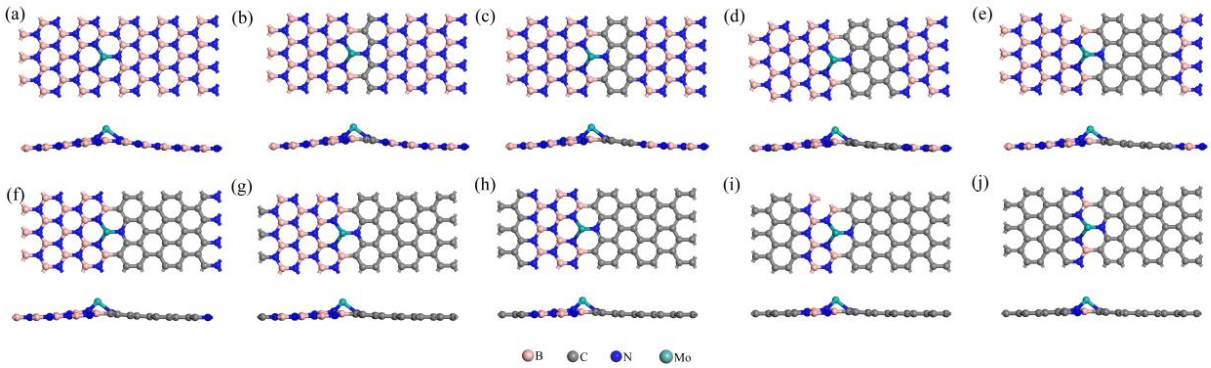

Fig. S11. The optimized structures of Mo@BCN-**n**. (a)-(f) represent Mo@BCN-0, Mo@BCN-1, Mo@BCN-2, Mo@BCN-3, Mo@BCN-4 , Mo@BCN-5, Mo@BCN-6, Mo@BCN-7 , Mo@BCN-8, and Mo@BCN-9, respectively.

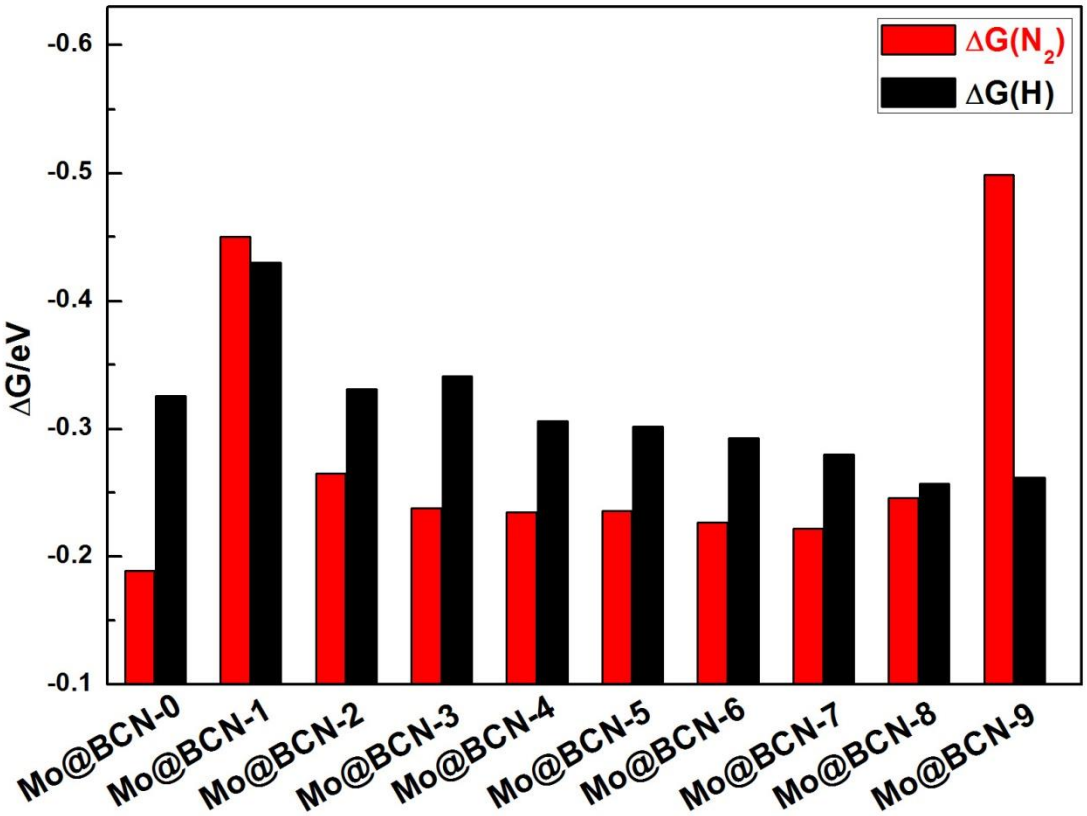

Fig. S12. The comparison of Gibbs free energies between N_2 and H adsorption on different models. Red and black pillars represent the $\Delta G(N_2)$ and $\Delta G(H)$, respectively.

(a)

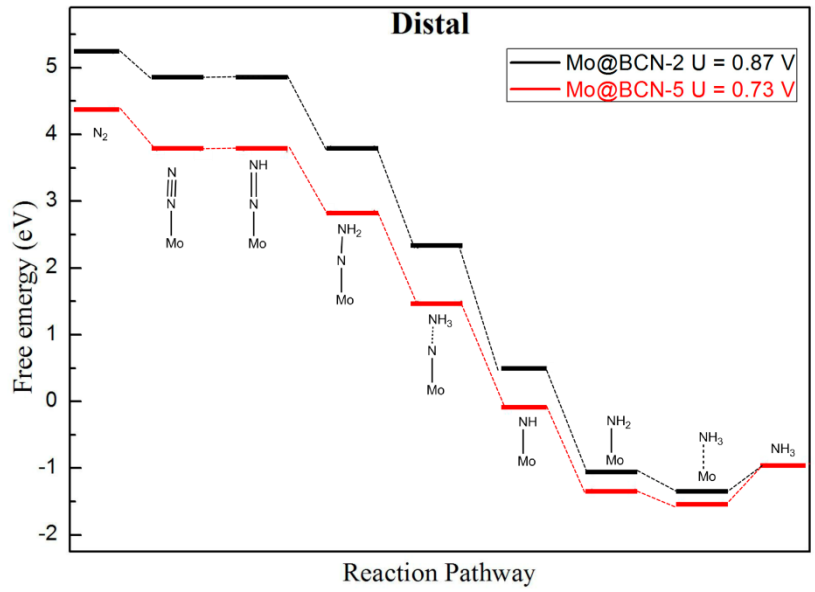
Distal
Mo@BCN-2 U = 0.87 V
Mo@BCN-5 U = 0.73 V
Free emergy (eV)
Reaction Pathway

(b)

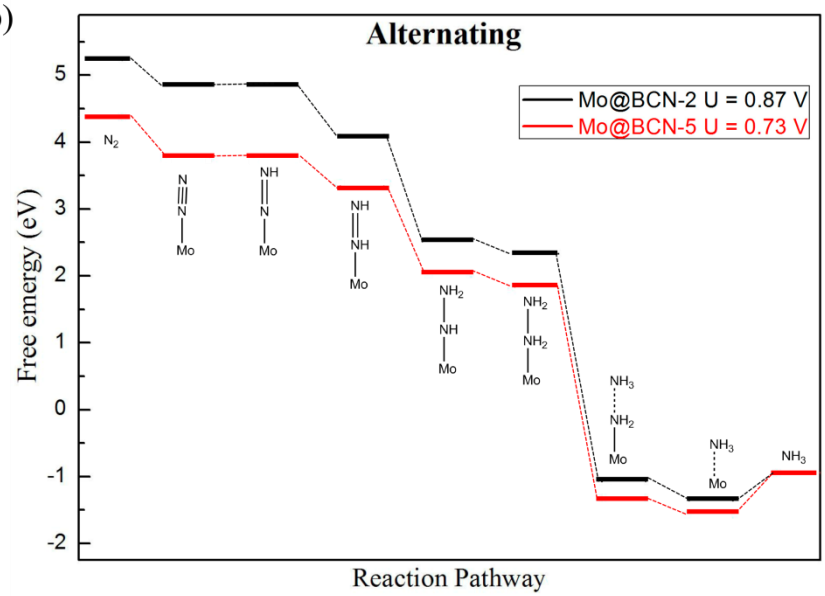
Alternating
Mo@BCN-2 U = 0.87 V
Mo@BCN-5 U = 0.73 V
Free emergy (eV)
Reaction Pathway

(c)

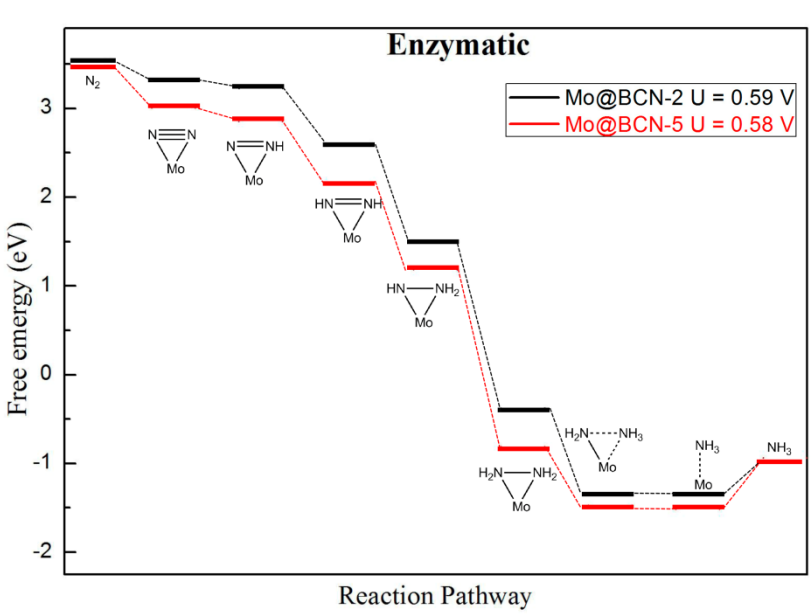
Enzymatic
Mo@BCN-2 U = 0.59 V
Mo@BCN-5 U = 0.58 V
Free emergy (eV)
Reaction Pathway

Fig. S13. Free-energy diagrams for the NRR on Mo@BCN-2 and Mo@BCN-5 through (a) distal, (b) alternating, and (c) enzymatic mechanisms at different applied potentials *vs* SHE.

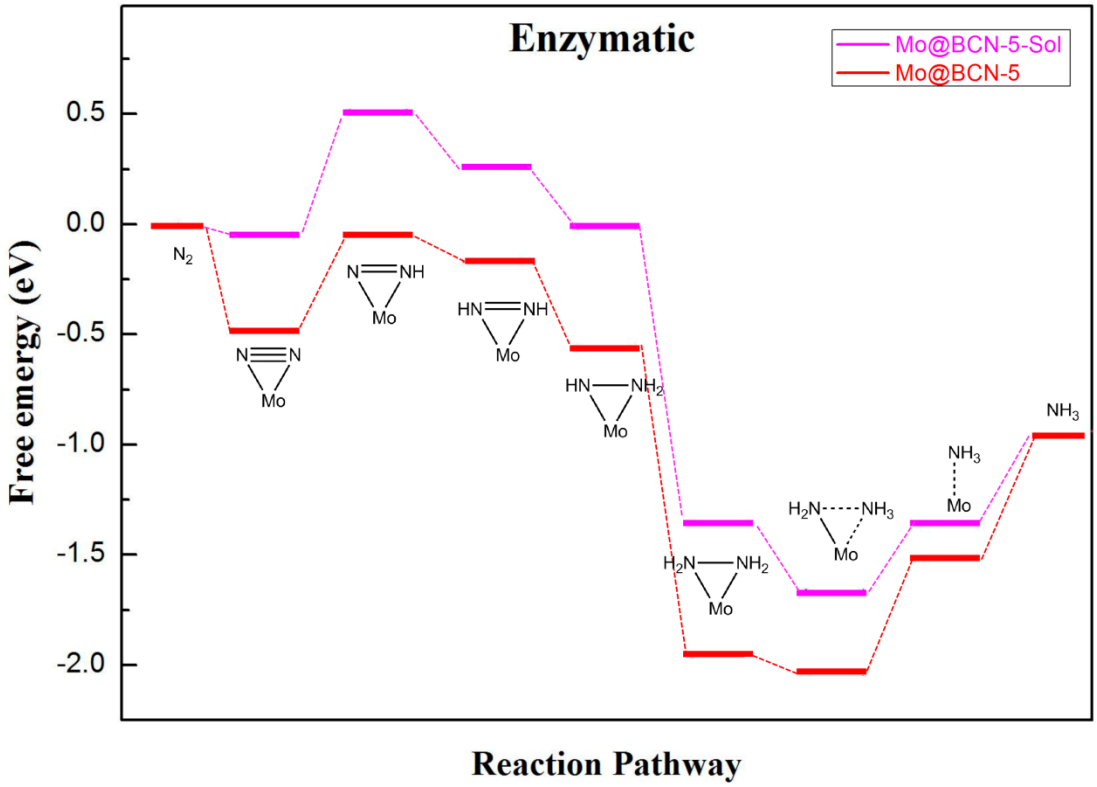

Fig. S14. Free-energy diagrams for the NRR on Mo@BCN-5 through enzymatic mechanisms with or without solvation effect.